D29

N79-20059

29

PROGRESS REPORT: SOME STEADY AND OSCILLATING AIRFOIL TEST RESULTS, INCLUDING THE EFFECTS OF SWEEP, FROM THE TUNNEL SPANNING WING

Franklin O. Carta and Arthur O. St. Hilaire
United Technologies Research Center

James B. Rorke and W. Donald Jepson
Sikorsky Aircraft Division
United Technologies Corporation

SUMMARY

A large scale tunnel spanning wing has been built and tested. The model can be operated as either a swept or unswept wing and can be tested in steady state or oscillated sinusoidally in pitch about its quarter chord. Data is taken at mid-span with an internal 6-component balance and is also obtained from miniature pressure transducers distributed near the center span region.

This paper presents a description of the system and a brief discussion of some of the steady and unsteady results obtained to date. These are the steady load behavior to Mach numbers of approximately 1.1 and unsteady loads, including drag, at a reduced frequency of approximately 0.1.

INTRODUCTION

It has long been recognized that conventional two-dimensional aerodynamic testing is not adequate for helicopter rotor blade applications. A typical section of the blade is simultaneously subjected to wide variations in Mach number, skew angle, and incidence angle, and all of these variations are both spatial and temporal. It is obvious that a traditional two-dimensional steady state test program can only satisfy a few of the quasi-steady needs of the designer, and even a sophisticated two-dimensional unsteady test is severely limited to incidence angle variations of the typical section. In recognition of this need for a test facility specifically geared to helicopter applications, United Technologies Corporation, through the combined efforts of its Sikorsky Aircraft Division and its Research Center (UTRC), has developed a minimum wall interference approach to obtaining airfoil aerodynamic data in the wind tunnel. Data are being obtained for both steady and unsteady pitching motions, both in oblique and conventional flow, over a wide range of Mach numbers and at representative full scale Reynolds numbers, using the same airfoil model and its associated measurement systems. The purpose of this paper is to present a brief description of the facility and its mode of operation and to discuss some of the results obtained to date.

HHH

SYMBOLS

Values are given in both SI and U.S. Customary Units. The measurements and calculations were made in U.S. Customary Units.

b	semichord, m
C_L, C_D, C_M	lift, drag, and pitching moment coefficient
C_N, C_c	normal and chord force coefficient
f	frequency, cycles/sec
k	reduced frequency
M	Mach number
r/R	span ratio
R_N	Reynolds number
V	velocity, m/sec
α	instantaneous incidence angle
α_M	mean incidence angle
$\Delta\alpha$	amplitude of motion
Λ	wing sweep angle
μ	rotor advance ratio
ψ	rotor azimuth angle
ω	frequency, rad/sec
$( )_N$	value taken normal to span
$( )_\infty$	free stream value

FACILITY DESCRIPTION

The wide range of parameter variations encountered in rotor craft is indicated by the plots in figs. 1 and 2. In fig. 1 a typical spanwise variation of lift coefficient as a function of Mach number for several blade attitudes (including hover) is superimposed on two operating conditions of concern to the designer, the drag divergence region and the potentially dangerous condition involving severe stall. (Note that the C_L peak near the blade tip in hover is caused by a trailing vortex encounter). Similarly, typical contours of constant skew angle (solid lines) and constant Mach number (dashed lines) are superimposed on a rotor disk in fig. 2. It is seen that the high load conditions are generally encountered at moderate Mach numbers on the retreating side of the disk, but that a need exists for high Mach number data as well. Furthermore, the effective blade sweep angle is zero only at azimuth angles of $\psi = 90^o$ and 270^o and is 15^o or greater over 60 percent of the rotor disk (as shown by the shaded region in fig. 2).

The first step in responding to these clearly defined needs was to build a versatile steady-state facility. The resulting Tunnel Spanning Wing system (TSW) was constructed by Sikorsky Aircraft in 1971. It consists of a basic tunnel spanning rectangular steel spar approximately 2.44 m (8 ft) in length, plus additional end pieces to complete the spar for installation at several available sweep angles or for installation in different wind tunnels with a test section that has one dimension at least 1.83 m (6 ft). Interchangeable airfoil-shaped shells with 40.64 cm (16 in) chord are mounted in sections onto the spar to provide the test configuration. A schematic view of this system is shown in fig. 3. It is seen that the model shell consists of two sets of pieces: the upper portions which surround the spar fore and aft, and the lower cover plates which complete the airfoil profile. Also shown in fig. 3 is the center span metric section, 20.32 cm (8 in) in width, which mounts to a pair of completely enclosed strain gage balances. This allows the airloads to be measured far from the tunnel side walls and ceiling. With this system it is possible to test several airfoil profiles in a single installation by replacing one set of model shells with another. The nominal chord length of 40.64 cm (16 in) allows data to be obtained at representative full scale Reynolds numbers and at a favorable tunnel height to chord ratio of 5.25 or greater for the tests conducted to date.

In addition to the internal balance in the metric section, two surface pressure tap systems are incorporated, arrayed principally in a chordwise direction. One system was originally installed along the centerline of the metric section to measure only steady state pressures for comparison with balance results. A second system was later installed in the model shell immediately adjacent to the metric section to measure both steady and oscillatory loads. As part of this system, some additional spanwise taps were included to measure spanwise loading and are so arrayed to relate the effects

of chordwise and streamwise surface pressure distributions when testing in oblique flow. Thus, the TSW incorporates dual airloads measurement systems which are redundant over a wide range of the test envelope and, together, are used as a data self-checking system. Hot film skin friction gages have also been included to assess the surface flow conditions in steady and oscillatory situations. A description of models and results of steady tests are presented in reference 1; the unsteady tests, not yet published, were performed by F. O. Carta at United Technologies Research Center (UTRC) under NASA Contract NAS 1-14873.

The TSW has been tested by the Navy and Sikorsky Aircraft in the NSRDC 2.13 m x 3.05 m (7ft x 10ft), 12 percent permeable transonic wind tunnel at zero sweep angle up to a maximum Mach number of M = 1.1 (ref. 1). The 3.06 m (10ft) span model installation is pictured in fig. 4. In this figure are shown a pair of part span supports from the tunnel floor to the model pressure surface. Tests with and without the struts installed showed conclusively that these supports had a negligible effect on the measured data. (The round object in the lower right corner of the tunnel was a part of the NSRDC sting mount system located several meters behind the TSW, and had no effect on the results). The Mach number/incidence angle and Mach number/Reynolds number envelopes achieved in these tests are shown in fig. 5. For comparison, a typical rotor envelope for a dive/pull-up maneuver is compared with the NSRDC M/α test envelope in the left panel, and the test range (dashed region) is compared with typical M/R_N variations for three helicopters in the right panel. It is believed that the test envelope represents some of the widest combinations of M and α achieved to date in a wind tunnel with a model having a full scale chord, and at conditions well above critical Reynolds number range.

A cooperative effort by UTRC and Sikorsky Aircraft has yielded the oscillatory system shown schematically in its unswept position in fig. 6. This system consists of a drive motor and transmission mounted beneath the UTRC 2.44 m (8ft) octagonal wind tunnel, which actuates a pair of push rods and oscillatory cranks to provide a sinusoidal motion of the model about its quarter chord (ref. 2). A swept, oscillating installation in the UTRC tunnel at $\Lambda = 30^{\circ}$ is pictured in fig. 7, looking upstream. In this test, one-third span supports were employed from both ceiling and floor of the tunnel to pivots located in the model spar. These were installed to overcome oscillatory bending deflections resulting from a small chordwise noncoincidence of model c.g. and pivot axis. (Note that the model was originally designed for steady testing only.) Steady-state oil flow studies have demonstrated that only a small portion of the airfoil surface area aft of the quarter chord was affected in the immediate vicinity of the supports, and that the effect on the center span flow was negligible. Oscillatory tests at $\Lambda = 30^{\circ}$ have been conducted at freestream Mach numbers as high as $M_{\infty} = 0.58$, and at reduced frequencies up to $k_N = b\omega/V\cos\Lambda = 0.1$ over a wide range of incidence angles and at amplitudes of $\pm$ 8 and $\pm$ 10 deg.

Testing was also conducted at $\Lambda = 45^{\circ}$ in steady state by Sikorsky Aircraft in the UTRC tunnel. This installation is pictured in fig. 8 as viewed from above. In this sequence of steady-state tests the model was subjected to a free stream Mach number as high as $M_{\infty} = 0.83$. or a normal to span Mach number of $M_N = M_{\infty}\cos\Lambda = 0.59$.

TEST RESULTS

A typical set of steady-state test results for the Sikorsky Aircraft SC-1095 airfoil are found in figs. 9, 10, and 11, obtained in the NSRDC tunnel (ref. 1). These figures contain the lift coefficient versus incidence angle, and the drag and pitching moment coefficients plotted as a function of lift coefficient for a wide range of Mach numbers from M = 0.3 to 1.075. The solid curves were obtained from balance measurements and the dashed curves are from integrated surface pressure and wake rake measurements. The flagged symbols represent repeat points. The internal balance measurement system was initially included for this type of testing to obtain drag data at high Mach numbers where compressibility effects preclude use of a wake rake. The several curves in each figure are plotted relative to a staggered set of origins, indicated by tic marks and zeroes along the left ordinate. The scale for the M = 0.3 curve is shown on the right ordinate. These figures show that all data exhibited excellent repeatability and data from both systems generally substantiated one another concerning the trends of he force coefficients with incidence angle and Mach number. The lift data from these separate measurement systems were in close agreement. The drag data from both systems were very similar, but at 0.9 Mach number the wake rake values were lower due to turbulent flow and/or compressibility effects. The pitching moment data from both systems were generally in agreement; however, at some conditions the balance coefficient data were more positive by + 0.015. After correcting for the differences in lift curve slope that occur between a ventilated and a solid wall wind tunnel, these data are in close agreement with the data obtained in UTRC 8 foot solid wall wind tunnel.

A few selected results from the unsteady UTRC tests are shown in figs. 12, 13, and 14 at $M_N = 0.3$ and 0.4 at $\Lambda = 0^{\circ}$ and 30°. Recalling figs. 1 and 2, it can be seen that these conditions are of primary importance to the rotor designer because they are representative of the flow experienced on the retreating side of the rotor disk where unsteady stall conditions are encountered. In figs. 12 and 13 the results were obtained from integration of the unsteady pressure distributions at each instant of time and in fig. 14 the loads were calculated from the unsteady output of the internal balances.

The effect of varying frequency at constant incidence is shown in fig. 12 for the unswept SC-1095 airfoil. Here a mean incidence angle of $\alpha_M = 12^o$ and an amplitude of $\pm 8^o$ produces periodic penetration of the stall regime, and as expected (refs. 3, 4, and 5), an increase in frequency causes a progressively larger overshoot of both normal force and moment in the dynamic stall regime . In fig. 13 sweep and oscillatory effects are combined. The solid lines represent the unswept configuration and the dashed lines the swept, both for a mean incidence angle of $\alpha_M = 15^o$ and an amplitude of $\pm 8^o$ (measured in the plane normal to the wing leading edge). Although a single sample such as this is insufficient to establish a trend, it is seen that the effect of sweep is to reduce the magnitude of the unsteady excursion through the dynamic stall regime (i.e., sweep appears to "soften" the impact of dynamic stall). It is also interesting to note that for unsteady conditions there is <u>not</u> a further extension of the maximum lift coefficient in oblique flow as is experienced in steady oblique flow.

Finally, fig. 14 shows unsteady lift and drag coefficient variations for the unswept wing at two mean incidence angles as obtained from the balance system. The significant observation to be made here is that, for the moderate Mach numbers tested, the unsteady drag is generally greater for increasing incidence angle and follows a clockwise loop in the high incidence regime, similar to that of the unsteady normal force. This behavior is easily explained by noting that the drag is made up of a vector sum of the normal and chord forces, expressed in component form as

$$C_D = C_N \sin\alpha - C_c \cos\alpha$$

For incidence angles in the range 15^o to 20^o the cosine is approximately three times the sine, but the normal force is at least 10 to 20 times the chord force. Consequently, the $C_N \sin\alpha$ term dominates the equation in the dynamic stall regime and the unsteady drag behaves as shown.

CONCLUDING REMARKS

The TSW concept has been used to demonstrate that a consistent airfoil data bank can be obtained at representative full-scale Reynolds numbers using the same model system for a wide variety of test conditions approaching those that are encountered by rotary wing aircraft. This model system provides a means to minimize wall interference effects and to eliminate the complicating factors introduced by using different airfoil models and load measuring systems required to cover this extensive aerodynamic environment, both steady and unsteady. This paper illustrates the versatility of this system with the few examples presented herein.

REFERENCES

1. Jepson, W. D: Two Dimensional Test of Four Airfoil Configurations with an Aspect Ratio of 7.5 and a 16 Inch Chord up to a Mach Number of 1.1. Sikorsky Engineering Report SER-50977, April 5, 1977, performed under Contract No. N60921-73-C-0057.

2. Carta, F.O. and A. O. St. Hilaire: An Experimental Study of Sweep Effects on the Unsteady Aerodynamics of a Pitching Airfoil. United Technologies Research Center Report R76-411931, March 1976.

3. Carta, F. O. and C. F. Niebanck: Prediction of Rotor Instability at High Forward Speeds. Vol. III. Stall Flutter. USAAVLABS Technical Report 68-18C, February 1969.

4. Liiva, J., F. J. Davenport, L. Gray, and I. C. Walton: Two-Dimensional Tests of Airfoils Oscillating Near Stall. USAAVLABS Technical Report 68-13, 1968.

5. Carr, L. W., K. W. McAlister, and W. J. McCroskey: Analysis of the Development of Dynamic Stall Based on Oscillating Airfoil Experiments. NASA TN D-8382, January 1977.

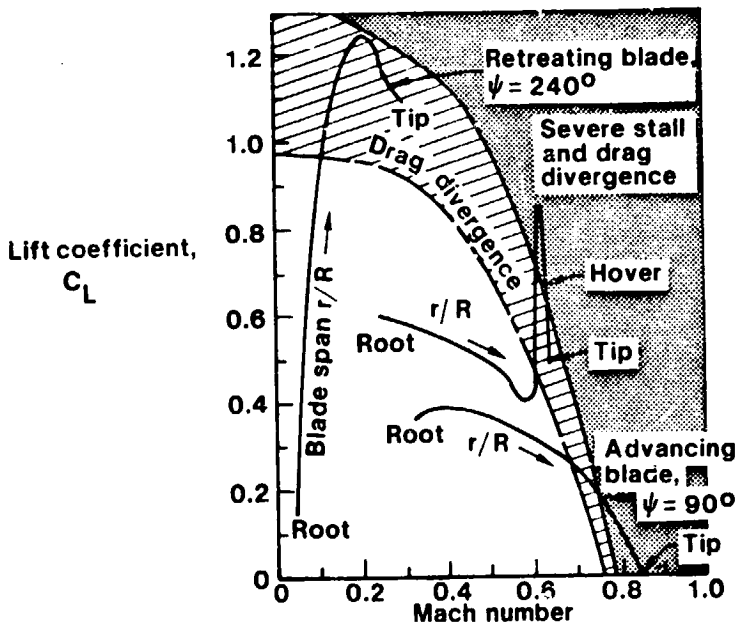

Figure 1.- Operating envelope.

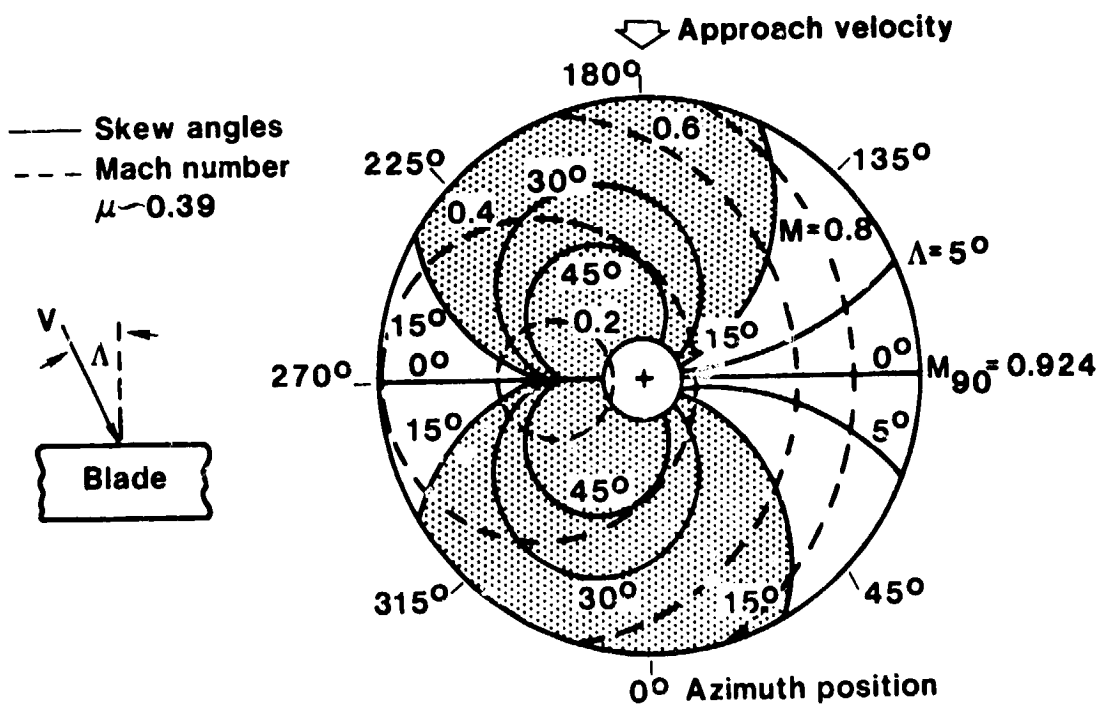

Figure 2.- Contours of skew angle and Mach number.

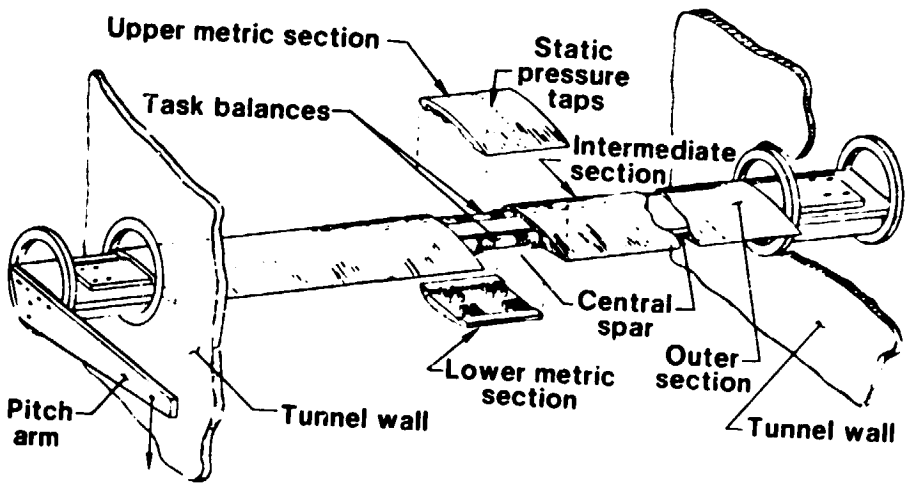

Figure 3.- Tunnel-spanning wing assembly.

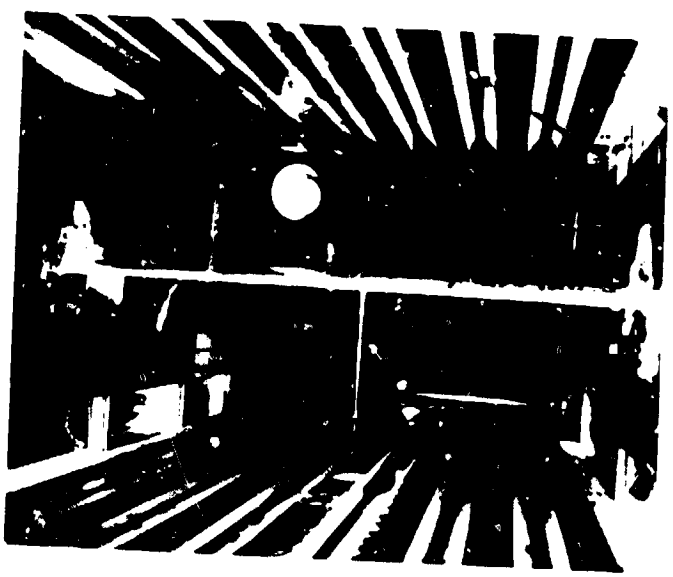

Figure 4.- NSRDC installation. $\Lambda = 0°$.

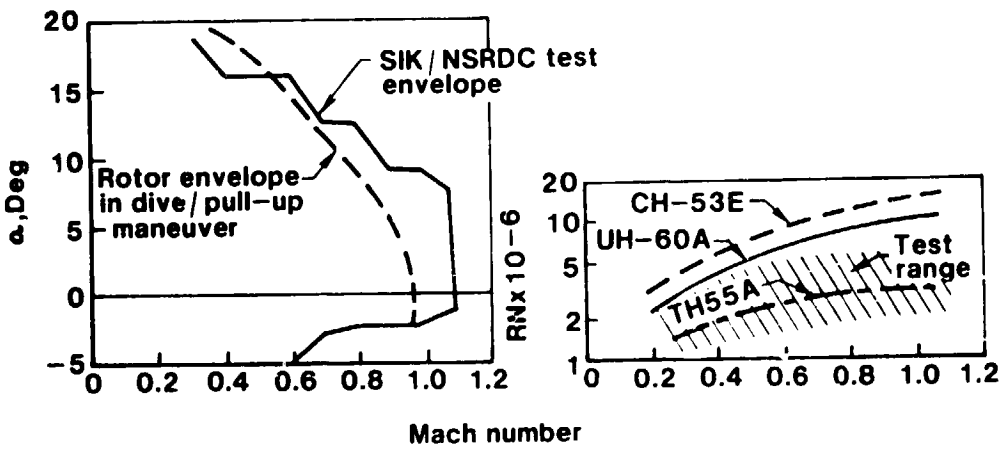

Figure 5.- Comparison of rotor and NSRDC test envelope. Steady state.

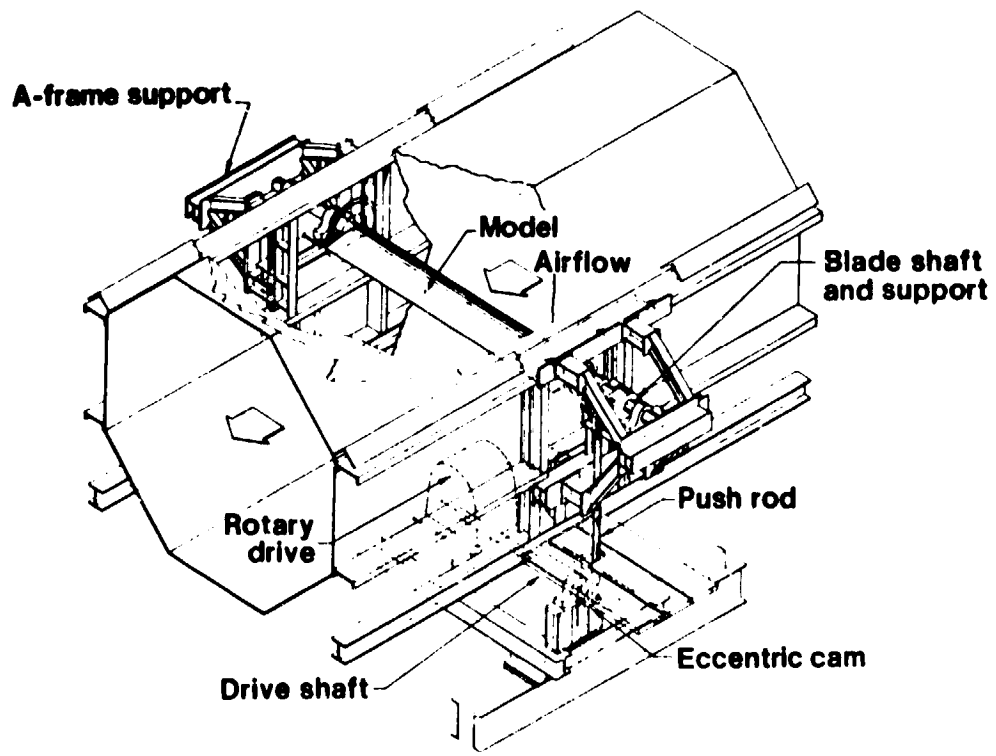

Figure 6.- UTRC main wind-tunnel oscillatory model system.

Figure 7.- UTRC installation. $\Lambda = 30°$.

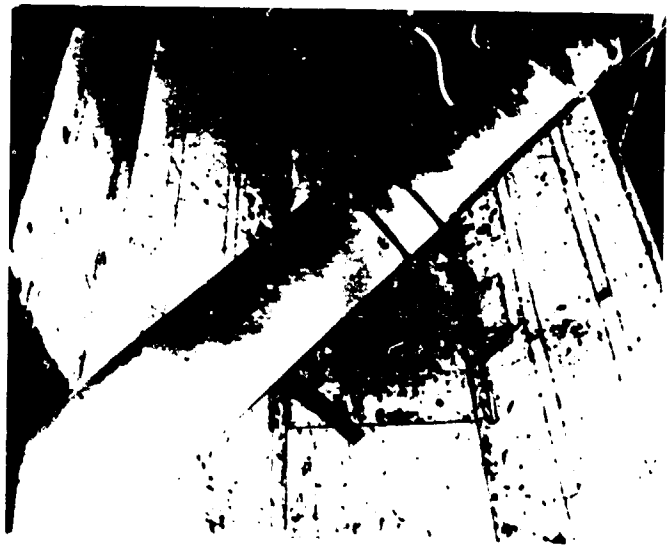

Figure 8.- UTRC installation. $\Lambda = 45°$.

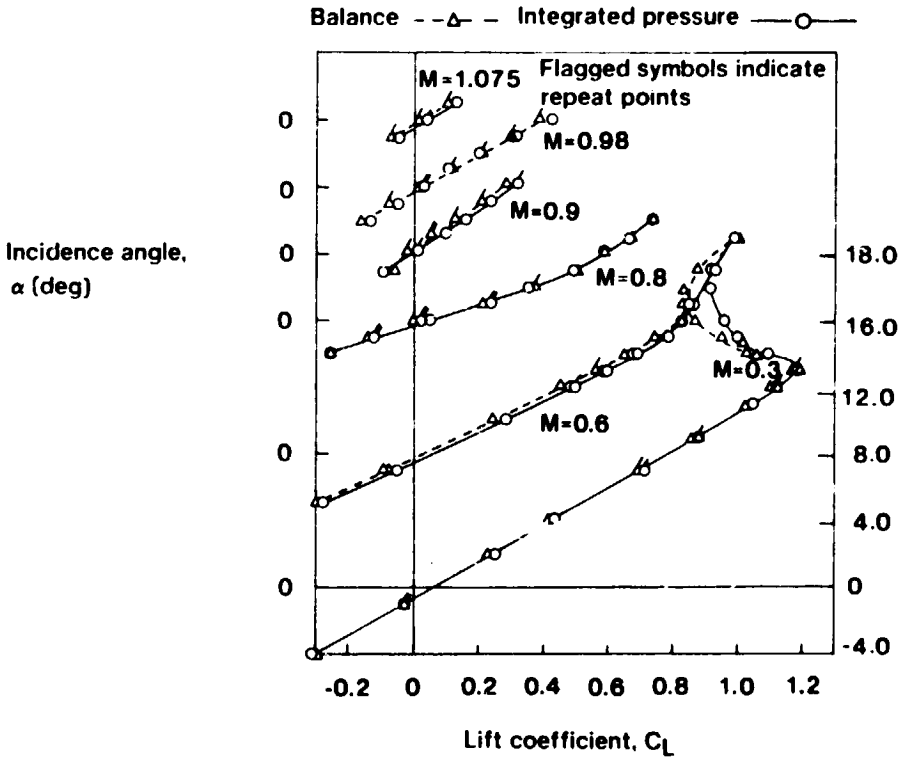

Figure 9.- Steady-state lift coefficient plotted against incidence angle.

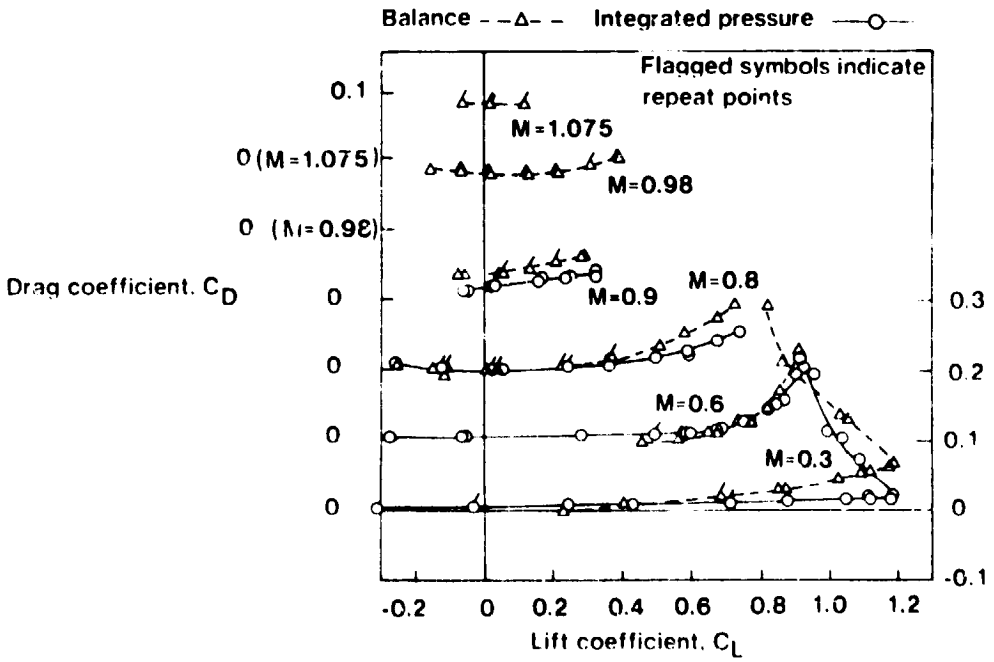

Figure 10.- Steady-state drag coefficient plotted against lift coefficient.

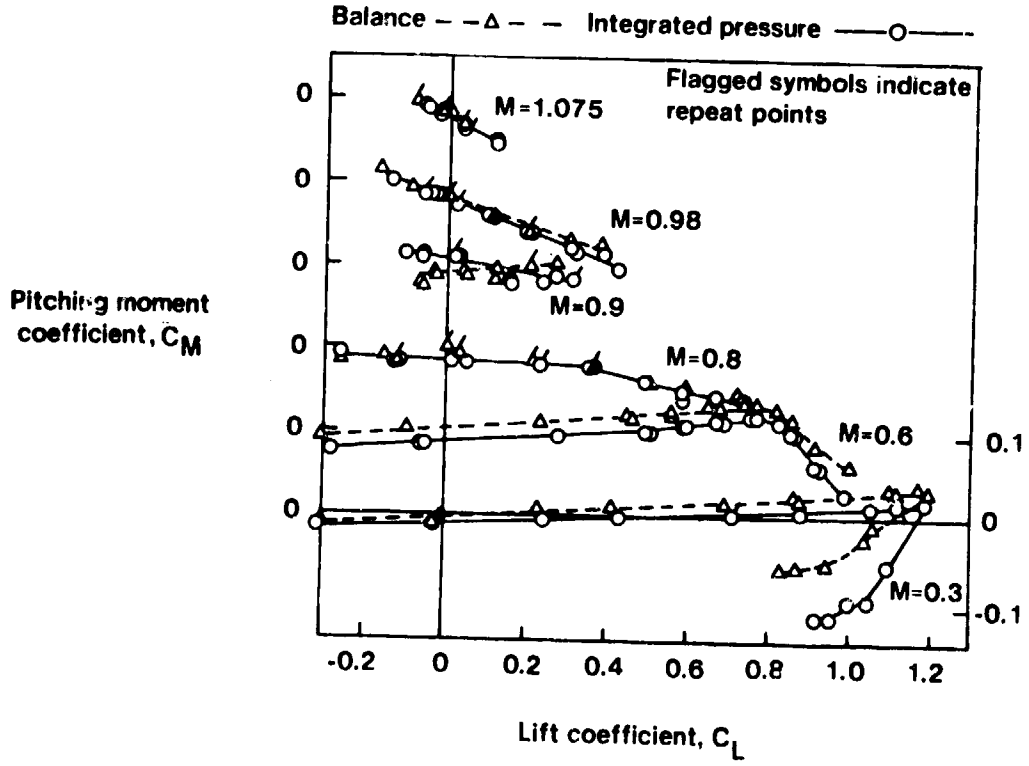

Figure 11.- Steady-state pitching-moment coefficient plotted against lift coefficient.

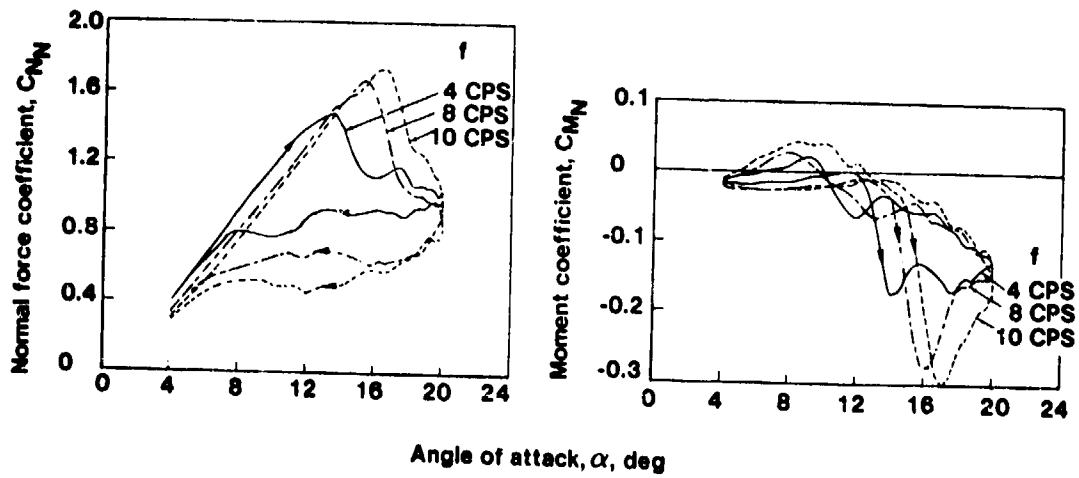

Figure 12.- Effect of frequency on oscillatory normal-force and moment coefficients from integrated pressures. SC-1095 airfoil; M = 0.4; $\Delta\alpha = \pm 8°$; $\alpha_M = 12°$

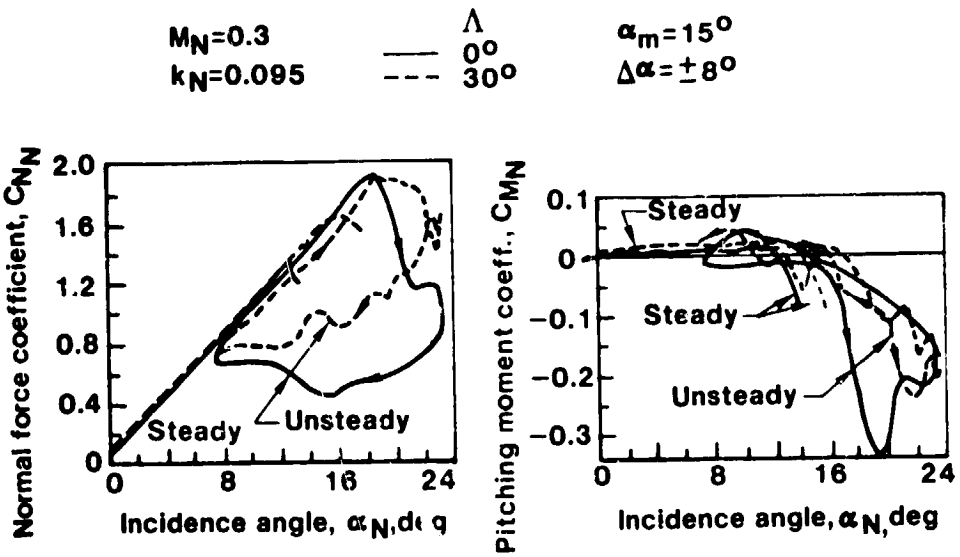

Figure 13.- Effect of sweep on oscillatory lift and moment coefficients from integrated pressures. SC-1095 airfoil.

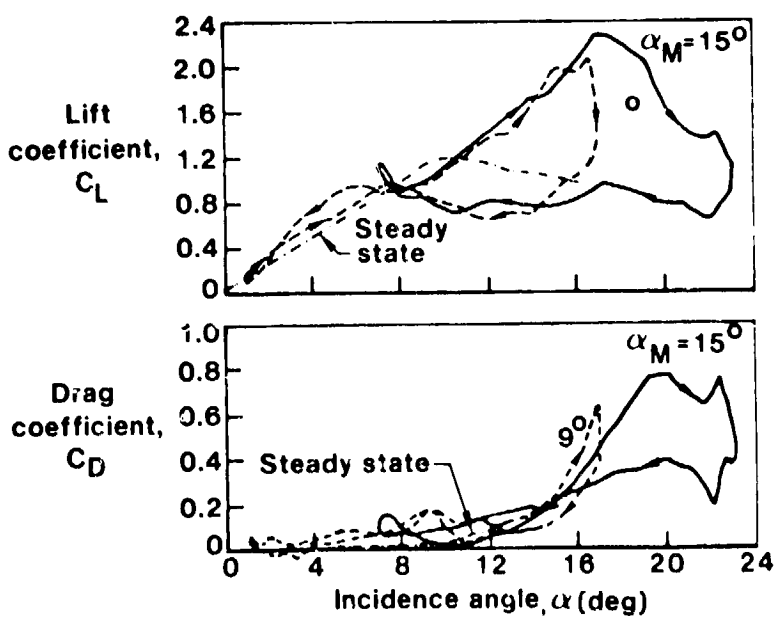

Figure 14.- Unsteady lift and drag coefficients from balance. SC-1095 airfoil; M = 0.3; Λ = 0°; Δα = ±8°; f = 3 cps; k = 0.096.